SCIENCE CHINA
Life Sciences

•RESEARCH PAPER•

February 2022 Vol.65 No.2: 295–308
https://doi.org/10.1007/s11427-020-1930-0

Single-cell RNA sequencing reveals Nestin$^+$ active neural stem cells outside the central canal after spinal cord injury

Muya Shu[1†], Xiaoyu Xue[1†], Hu Nie[1], Xianming Wu[1], Minghan Sun[1], Lianyong Qiao[1], Xing Li[3], Bai Xu[1], Zhifeng Xiao[1], Yannan Zhao[1], Yongheng Fan[1], Bing Chen[1], Jixiang Zhang[1], Ya Shi[1], Yaming Yang[1], Falong Lu[1,2*] & Jianwu Dai[1,2*]

[1]*State Key Laboratory of Molecular Developmental Biology, Institute of Genetics and Developmental Biology, Chinese Academy of Sciences, Beijing 100080, China;*
[2]*University of the Chinese Academy of Sciences, Beijing 100101, China;*
[3]*Key Laboratory of Organ Injury, Aging and Regenerative Medicine of Hunan Province, Changsha 410008, China*

Received February 13, 2021; accepted March 15, 2021; published online May 28, 2021

Neural stem cells (NSCs) in the spinal cord hold great potential for repair after spinal cord injury (SCI). The ependyma in the central canal (CC) region has been considered as the NSCs source in the spinal cord. However, the ependyma function as NSCs after SCI is still under debate. We used Nestin as a marker to isolate potential NSCs and their immediate progeny, and characterized the cells before and after SCI by single-cell RNA-sequencing (scRNA-seq). We identified two subgroups of NSCs: the subgroup located within the CC cannot prime to active NSCs after SCI, while the subgroup located outside the CC were activated and exhibited the active NSCs properties after SCI. We demonstrated the comprehensive dynamic transcriptome of NSCs from quiescent to active NSCs after SCI. This study reveals that Nestin$^+$ cells outside CC were NSCs that activated upon SCI and may thus serve as endogenous NSCs for regenerative treatment of SCI in the future.

neural stem cell, Nestin, scRNA-seq, Smart-seq2, ependymal cell

Citation: Shu, M., Xue, X., Nie, H., Wu, X., Sun, M., Qiao, L., Li, X., Xu, B., Xiao, Z., Zhao, Y., et al. (2022). Single-cell RNA sequencing reveals Nestin$^+$ active neural stem cells outside the central canal after spinal cord injury. Sci China Life Sci 65, 295–308. https://doi.org/10.1007/s11427-020-1930-0

INTRODUCTION

Tissue injury triggers cell proliferation for repair, which is critical for the survival of organisms. The newly generated cells seal the damaged area and replace the lost cells to maintain organ function. In the central nervous system (CNS), injury leads to neural stem cells (NSCs) proliferation and generates neural and non-neural cells. Understanding the injury induced activated NSCs may help to identify and take advantage of NSC sources in CNS.

The ependyma in the central canal (CC) region was believed to host the NSCs in adult spinal cord for a long time (Hamilton et al., 2009; Hugnot and Franzen, 2011; Meletis et al., 2008). These NSCs are in low proliferate rate to self-renew under normal conditions, but they show the potential to produce astrocytes and oligodendrocytes after spinal cord injury (SCI). The protein Foxj1 has been used as a spinal cord ependymal cells marker, which marked the ependymal cells located in the CC, but studies using different Foxj1 lineage-tracing mice have obtained varying results (Devaraju et al., 2013; Jacquet et al., 2009; Li et al., 2018a; Muthusamy et al., 2018; Shah et al., 2018). The ependymal cells from human Foxj1-CreERT promoter line have been proposed as a major population of NSCs that give rise to glial cells that participate in scar formation after SCI (Barnabé-Heider et al.,

†Contributed equally to this work
*Corresponding authors (Jianwu Dai, email: jwdai@genetics.ac.cn; Falong Lu, email: fllu@genetics.ac.cn)

2010). This view has been questioned by tracing with the knock-in Foxj1^{CreERT2} line, which showed that the contribution of Foxj1^{+} cells to scar-forming is limited (Muthusamy et al., 2014; Ren et al., 2017). Moreover, clinical samples from patients with SCI were negative for Ki67 or MCM2 staining at CC, suggesting that CC cells lacked proliferation ability (Paniagua-Torija et al., 2018). Contradictory conclusions on the stemness of the ependyma have also been found in brain researches (Habib et al., 2016; Luo et al., 2015; Mirzadeh et al., 2008; Muthusamy et al., 2018; Shah et al., 2018). Although whether ependymal cells are NSCs is controversial, these studies suggest the existence of another source of NSCs in spinal cord besides CC cells.

Nestin is a type VI intermediate filament protein and has been used as a common marker of NSCs/neural progenitor cells (NPCs) in CNS (Bernal and Arranz, 2018). Previous research in spinal cord found Nestin^{+} cells were located in the CC region (Nomura et al., 2010). The Nestin^{+} cells from the CNS can form neurospheres under proper culture conditions *in vitro* and are able to differentiate into astrocytes, oligodendrocytes and neurons (Barnabé-Heider et al., 2010; Meletis et al., 2008). After SCI, the expression of Nestin is increased in the ependyma of the spinal cord (Bernal and Arranz, 2018; Cawsey et al., 2015; Li et al., 2017).

After SCI, NSCs in spinal cord immerse in a complex niche, mixed with their progeny at distinct developmental stages. Comprehensive analysis of NSCs and their progeny biologic mechanism after SCI requires elaborate information from quantification of molecular properties, such as dynamic changes of transcriptome. Traditional approaches "normalized" cells, which cannot reflect the heterogeneity of cells within the tissue (Grün and van Oudenaarden, 2015). It also failed to trace the transcriptome dynamic changes of NSCs after SCI *in vivo*. Single-cell RNA sequencing (scRNA-seq) can solve these two challenges. It profiles gene expression of individual cells and thus decoded single cell molecular profiles which were masked by population level analysis. Moreover, the traditional systems only use a few of known markers to define the dynamic process, while scRNA-seq maps out the developmental trajectory of NSCs at high resolution using an unbiased profile of molecular features of cellular states. Through this cutting-edge technique, we can draw a dynamic single-cell transcriptome blueprint of NSCs after SCI.

To bypass the controversy of NSCs property of Foxj1 cells and capture the potential NSCs in spinal cord of adult mice, we used Nestin-GFP genetic labeling system to label NSCs and traced their fate during the acute injury phase (5 days post injury, pdi) (Yamaguchi et al., 2000). We applied scRNA-seq to analyze fluorescence-activated cell sorting (FACS)-purified Nestin-GFP^{+} cells from adult mice at 0 pdi (un-injured sample) and 5 dpi. Our study revealed the dynamic systematic molecular characterization of adult spinal cord NSCs after SCI *in vivo*. Unsupervised bioinformatics analysis identified two groups of Nestin-GFP^{+} cells in the spinal cord: one along with the CC and the other outside the CC. After SCI, the Nestin-GFP^{+} cells along CC remained quiescent, however, the Nestin-GFP^{+} cells outside CC gained activated NSCs (aNSCs) properties, including augmented translation and oxidative phosphorylation capacity. Our data indicate that the cells outside the CC acted as the aNSCs after SCI and possessed the ability to differentiate from other cell types. These findings may help us to further understand NSCs in the spinal cord, which provide a guideline to manipulate the NSCs source and boost the functional performance of clinical therapy in future regenerative research and practice.

RESULTS

Nestin-GFP^{+} cells are quiescent in the intact spinal cord

To seek the spinal cord NSCs and elucidate details of molecular dynamics of these cells immediately after SCI, we took advantage of Nestin-GFP transgenic mouse line (Shin et al., 2015; Yamaguchi et al., 2000) that can trace the Nestin^{+} cells fate over a short time (Shin et al., 2015). We observed the GFP expression pattern of the transgenic mice in the spinal cord by immunofluorescence. Consistent with previous studies, the immunofluorescence results using antibody specific to GFP showed that Nestin-GFP labeled cells were mainly located in the CC (Figure 1A). Interestingly, a few Nestin-GFP^{+} cells were also detected outside the CC (longitudinal sections, 31.33±2.33 Nestin-GFP^{+} cells per 100 μm, n=3) (Figure 1A). Transverse sections exhibited fewer Nestin-GFP^{+} cells present outside compared with within the CC, and the cells were mainly located in the grey matter region (37.33±2.60 Nestin-GFP^{+} cells per section, n=3) (Figure 1A, right). Similar to the cells located within the CC, the Nestin-GFP^{+} cells outside the CC had two long processes (Figure 1B–D). Astrocytes and pericytes also expressed Nestin in the intact spinal cord (Bernal and Arranz, 2018; Göritz et al., 2011). To exclude the possibility that the observed Nestin-GFP^{+} cells were astrocytes, we detected the expression of glial fibrillary acidic protein (GFAP, a well-known marker for astrocytes) in Nestin-GFP^{+} cells. Most of GFAP^{+} cells were near GFP^{+} cells in the CC, and only a few cells were GFAP^{+}GFP^{+} (GFAP^{+}GFP^{+} cells/CC GFP^{+} cells, approximately 6.06%) (Figure 1D), consistent with the characteristics of ependymal cells in the CC (Sabelström et al., 2014). However, the cells outside of the CC were negative for GFAP (Figure 1B), suggesting that astrocytes contributed minimally to Nestin-GFP^{+} cells in adult Nestin-GFP mice. We also examined the proliferation ability of Nestin-GFP^{+} cells in intact spinal cord under normal condition. Only a few of Nestin-GFP^{+} cells stained with Ki67 (approximately

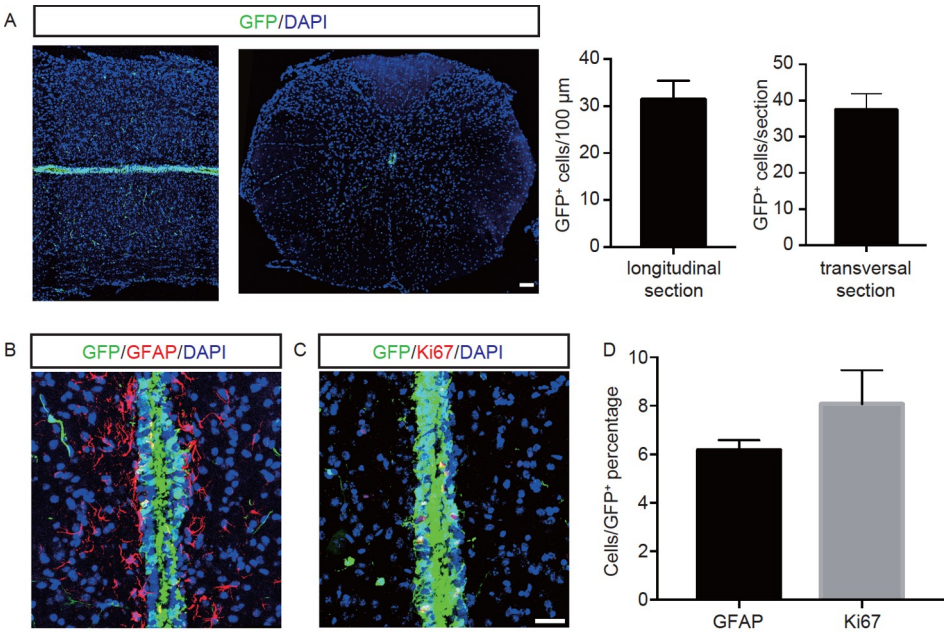

Figure 1 Distribution of Nestin-expressing cells in intact spinal cord in adult Nestin-GFP mice. A, Nestin expression cells are identified by GFP immunofluorescence. (Left) Longitudinal section showing GFP$^+$ cells (green) lines along with the CC, with some cells outside the CC. (Right) Transversal section of Nestin-GFP mice showing GFP$^+$ cells (green) locate in CC. Scale bars, 100 μm. B–D, Validation of quiescent status of GFP$^+$ cells by immunofluorescence. B, GFP$^+$ cells (green) are closely associated with GFAP$^+$ cells in CC (red), the GFP$^+$ cells outside the CC are GFAP- cells. C, Longitudinal section stained with GFP (green) and Ki67 (red). Spare of GFP$^+$ cells are GFP and Ki67 co-immunoreactivity. D, The percentage of GFP$^+$ cells with GFAP or Ki67 immunostaining. Scale bars, 50 μm.

8.16% Ki67 cells/CC GFP$^+$ cells) (Figure 1D and E). This result indicated that Nestin-GFP$^+$ cells were mostly quiescent in the intact spinal cord.

Nestin$^+$ cells are activated after spinal cord injury

Next, we investigated the response of Nestin-GFP$^+$ cells after SCI. Mice were randomly divided into two groups. One group received a 1 mm midline incision at the level of T8–T10 of the spinal cord, and spinal cords were collected the at 5 pdi. This group of samples was referred as 5 pdi samples. Another group of un-injured samples was referred as 0 pdi samples. Compared with the number of GFP$^+$ cells in the intact spinal cord, GFP$^+$ cells expanded near the lesion area at 5 pdi (Figure 2A). Qualitative analysis within 1 mm rostral and caudal to the lesion site of the spinal cord showed an increase in the proportion of Nestin-GFP$^+$ cells from approximately 8.52% to 13.75%. Nestin-GFP$^+$ cells also exhibited dramatic morphology changes around the lesion area after SCI. At 0 dpi spinal cord, these cells protruded two long and thin processes, which were similar to radial glial cells (Figure 2B). However, near the lesion core, some of Nestin-GFP$^+$ cells underwent shape transformation by 5 pdi. The shapes of these cells were varied, but all exhibited two common features, hypertrophy and thickening process (Figure 2B).

Then, we investigated the origin of the newly appeared Nestin-GFP$^+$ cells at 5 pdi after SCI. If Nestin-GFP$^+$ cells in the CC are the source of NSCs, they would be activated and proliferated after SCI, migrated to the lesion site and participated in scar formation (Barnabé-Heider et al., 2010; Meletis et al., 2008). This would likely result in a gradient concentration of Nestin-GFP$^+$ cells along with the CC, with the CC area containing more Nestin-GFP$^+$ cells than the area outside of the CC. However, no such gradient pattern was detected (Figure 2A and B). In contrast, the decreasing density of Nestin-GFP$^+$ cells was observed along the distance from the lesion site. The results indicated that the newly appeared Nestin-GFP$^+$ cells outside the CC likely originated from outside the CC rather than from Nestin-GFP$^+$ cells in the CC. We tested this hypothesis by using bromodeoxyuridine (BrdU) assay. Mice were injected with BrdU immediately after SCI and repeated every 6 h for 3 d (Figure 2C). Remarkably, Nestin-GFP$^+$ cells were labeled with BrdU at 5 pdi (Figure 2D) (Ren et al., 2017). Nestin-GFP$^+$ cells outside the CC had a higher proliferation rate than the cells in the CC near the lesion location (Figure 2E). This finding suggested that Nestin-GFP$^+$ cells possessed proliferation ability after SCI.

Single cell transcriptomics of Nestin-GFP$^+$ cells after SCI

To understand the dynamics of Nestin-GFP$^+$ cells at the molecular level during the acute phases after SCI *in vivo*, we performed scRNA-seq using Nestin-GFP$^+$ cells isolated from

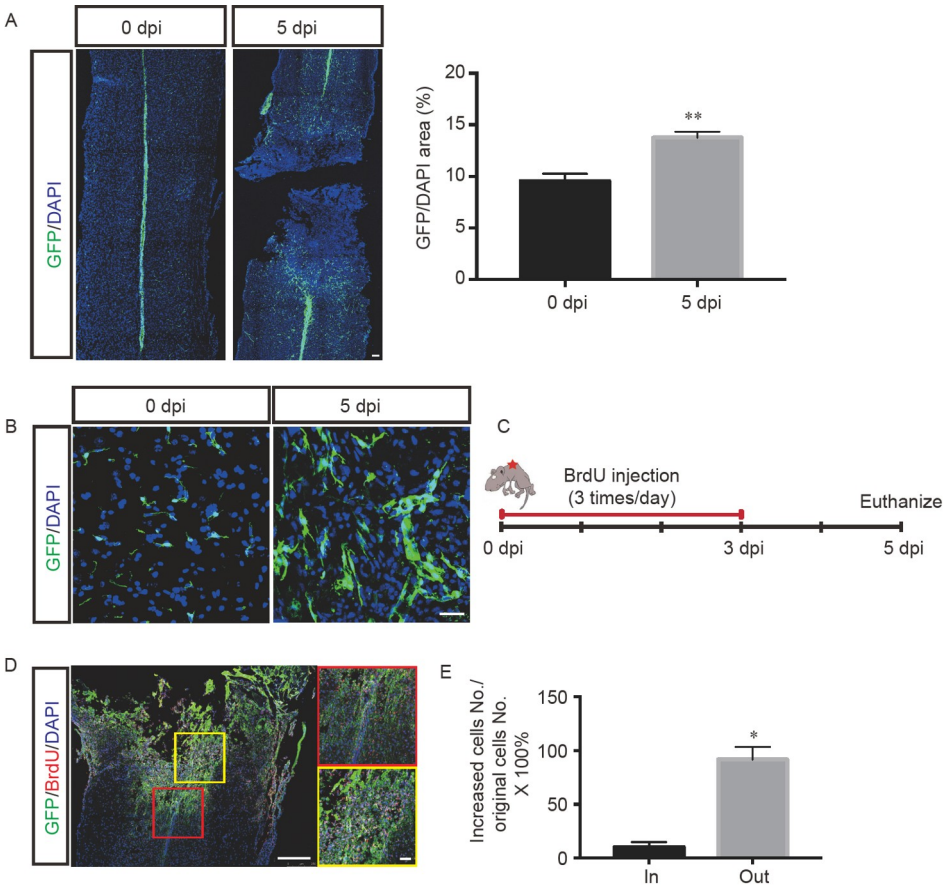

Figure 2 NSCs are activated after SCI. A, GFP$^+$ cells were increased in the acute phase after SCI. (Left) Distribution of GFP$^+$ cells (green) before SCI in adult Nestin-GFP mice. (Right) Distribution of GFP$^+$ cells (green) at 5 pdi of SCI in adult Nestin-GFP mice. The histogram shows the quantification of the GFP$^+$ area (green)/DAPI area (blue). *, P<0.05; **, P<0.01; Student's t test. Scale bars, 100 μm. B, Morphology of GFP$^+$ cells. (Left) The morphology of GFP$^+$ cells (green) outside of the CC at 0 pdi. The cells were characterized by two long extending processes. (Right) The morphology of GFP$^+$ cells (green) adjacent to the lesion site at 5 pdi. The GFP$^+$ cells (green) exhibited hypertrophy and thickening process. Scale bars, 50 μm. C, A schematic diagram of BrdU injection. Mice were injected with BrdU every 6 h for 3 d after SCI. D and E, Validation of the proliferation ability of GFP$^+$ cells. Immunoreacitivity was detected at 5 pdi in longitudinal sections. BrdU (red) staining in spinal cord at 5 pdi showed that GFP$^+$ (green) cells in and outside the CC were proliferated after SCI. Cells in both locations have the proliferation property of NSCs. Red square presented the GFP$^+$ cells in the CC area. Yellow square presented the GFP$^+$ cells outside of the CC area. *, P<0.05; **, P<0.01; Student's t test. Left scale bars, 250 μm, Right scale bars, 50 μm; In: cells in CC; Out: cells out of CC.

Nestin-GFP mice at 0 and 5 pdi by FACS. scRNA-seq libraries were constructed for each cell via Smart-seq2 strategy (Figure 3A) (Picelli et al., 2014). We performed two independent batches of scRNA-seq experiments (batch 1: 145 cells from 0 pdi and 132 cells from 5 pdi samples; batch 2: 73 cells from 0 pdi and 137 cells from 5 pdi samples). Both sets of data showed similar results (Figure S1 in Supporting Information). The sequencing metrics for the pooled library and quality control measures indicated that the libraries were of good quality (Figure S1 in Supporting Information). Reads were evenly distributed throughout the whole span of transcripts. Low-quality cells with <300 detected genes and cells with >12,000 detected genes were excluded (Figure S1 in Supporting Information). We obtained a total of 474 scRNA-seq datasets with good quality. To catalog the major cell types of the 0 and 5 pdi Nestin-GFP$^+$ cells, we performed Uniform Manifold Approximation and Projection (UMAP) analysis using Seurat3 and identified 3 subclusters: 0, 1 and 2. Notably, cluster 0 and cluster 1 groups could not be clearly segregated on the plot of principal component analysis (PCA) (Figure 3B), but nearly all of the cluster 1 cells were from 5 pdi samples. The results of two biological replicates over two-time points were concordant (Figure S2 in Supporting Information).

To classify each cell cluster unbiasedly, we identified three subclusters by gene ontology (GO) analysis of the differentially expressed genes (Figure 3C). The cluster 0 enriched in a number of markers identified in quiescent NSCs (qNSCs), including *Sox9*, *S100b*, *Clu*, *Gja1* and *Id4* (Figure 3C; Figure S3A in Supporting Information) (Dulken et al., 2017; Llorens-Bobadilla et al., 2015; Shah et al., 2018). This cluster also expressed ependymal markers, such as *Ccdc153*, *Mia*, *Foxj1* and *Tm4sf1* (Figure 3; Figure S3A in Supporting Information), in accordance with previous reports indicating that qNSCs shared a number of genes with the ependyma (Chen et al., 2017; Shah et al., 2018). Although the cluster 1

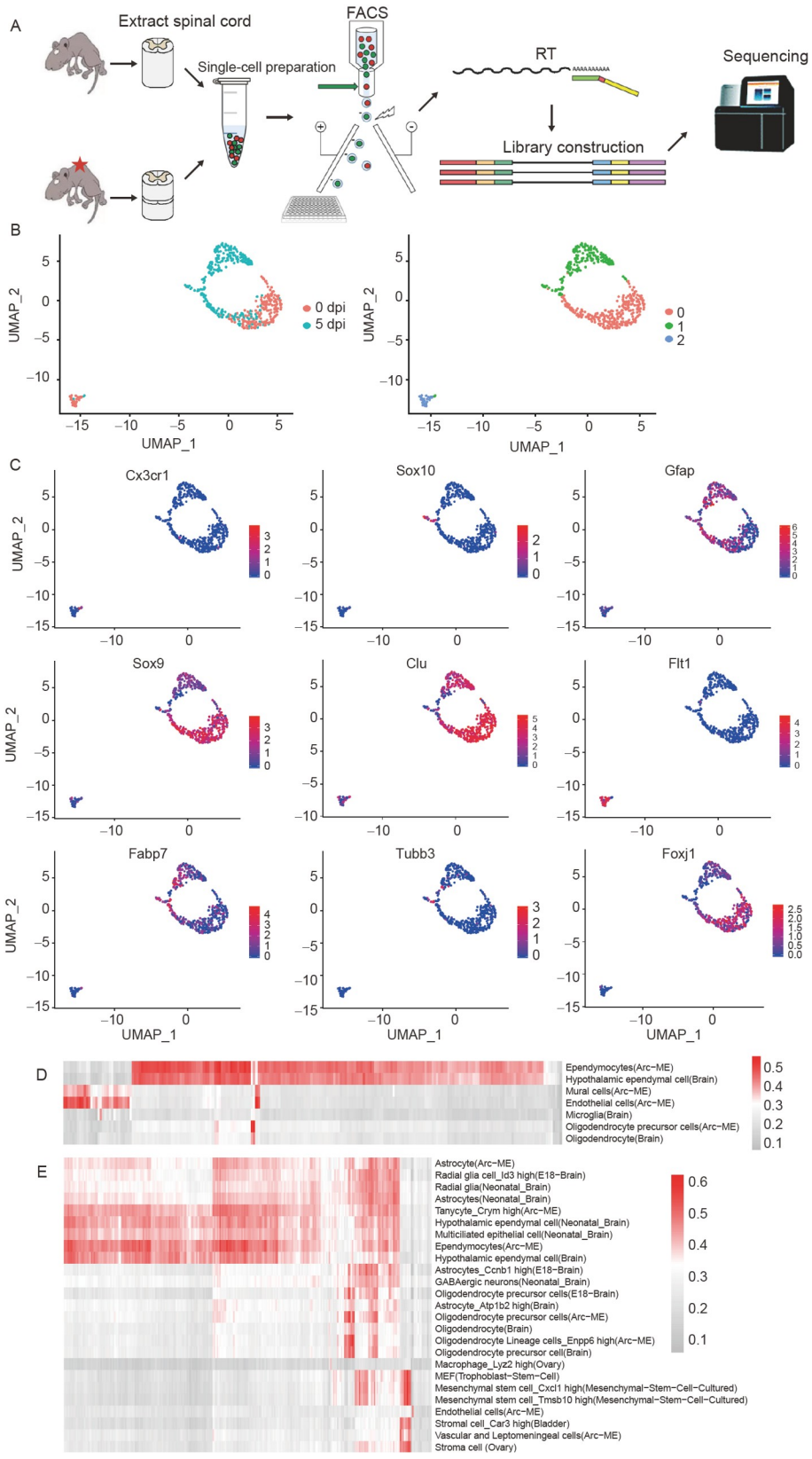

Figure 3 scRNA-seq analysis of Nestin-GFP$^+$ cells after SCI. A, Flowchart of scRNA seq. Nestin-GFP mice were sacrificed to isolate GFP$^+$ cells via FACS. Then using Smart2-seq strategy to construct libraries. B, PCA plot shows that the Nestin-GFP$^+$ cells were clustered into three populations. (Left) 0 and 5 pdi Nestin-GFP$^+$ cells in the PCA plot. C, Gene expression profiles of selected marker genes. D and E, MCA analysis of 0 and 5 pdi Nestin$^+$ cells. The *X*-axis indicates the single cells which were analyzed. The *Y*-axis indicates the cell type in MCA. The 0 pdi cells show high similarity to ependymal cells (D). Some of 5 pdi cells remain characteristics of ependymal cells, but some show the intermediate status to other types of cells (E).

group still expressed *Sox9*, *S100b* and *Clu*, the expression levels were much lower than those in cluster 0. The cluster 1 group highly expressed the previously reported aNSCs marker *Rpl32* (Figure S3B in Supporting Information) (Dulken et al., 2017). The aNSCs markers *Cdk1* and *Ccna2*, which are related to the cell cycle pathway were also detected in these 5 pdi Nestin-GFP$^+$ cells (Figure S3B in Supporting Information).

The small bunch of cluster 2 cells was enriched with endothelial markers, such as *Cd34* and *Flt1* (Figure 3C; Figure S3C in Supporting Information). We also detected some other markers in Nestin-GFP$^+$ cells, however, the expressions of oligodendrocyte progenitor cells (OPCs) maker *Sox10*, microglia marker *Cx3cr1* and neuron marker *Tubb3* in these cells were quite low or even undetectable (Figure 3C). Cluster 2 cells were therefore defined as endothelial cells.

To reveal the diversity of Nestin$^+$ cells during SCI, we uploaded our data and referenced with the Mouse Cell Atlas (MCA) database (http://bis.zju.edu.cn/MCA/). Comparison of the scRNA-seq dataset with the MCA database showed that 0 pdi Nestin-GFP$^+$ cells were highly homogenous (Figure 3D). Their gene expression pattern conformed to the ependymal cell type in MCA database, except for the cluster 2 cells, which fitted into endothelia. The heterogeneity of Nestin-GFP$^+$ cells increased at 5 pdi. Approximately half of the cells retained ependymal cell characteristics. The other half of the cells began to at the intermediate states of turning into other cell types, including astrocytes, radial glia cells, neurons and oligodendrocytes, however, these cells still exhibited largely the ependymal cell like properties (Figure 3E). Comparison of 5 pdi cells with those in the MCA database demonstrated several types of cell identities suggesting their multipotency, while the multi-phase of the cells suggested intermediate states in the continuum between Nestin-GFP$^+$ cells and their immediate progeny.

Based on classical marker expression analysis, MCA analysis, and the top 15 markers in each cell population (Figure S4A in Supporting Information), the three clusters were assigned into qNSCs (cluster 0), aNSCs (cluster 1) and endothelial cells (cluster 2). Although analysis of endothelial cells would be interesting (Klein et al., 2003), we focused on the NSCs properties of Nestin-GFP$^+$ cells in this study and therefore did not investigate the endothelial cells further. Based on these observations, we concluded that after SCI, qNSCs were activated to proliferate after SCI and initiated the process to differentiate into different lineages, including astrocytes, radial glia cells, neurons and oligodendrocytes.

Nestin-GFP$^+$ cells are primed to aNSCs at 5 pdi after SCI

MCA analysis indicated that the plasticity of Nestin-GFP$^+$ cells was increased after SCI. We therefore sought to validate the reliability of our analysis and the plasticity of Nestin-GFP$^+$ cells after SCI. The top 12 variable genes of aNSCs are shown in Figure 4A. *Rpl13a*, *Rps15a* and *Rpl22l1* are important genes for ribosomal biogenesis, and were upregulated in aNSCs. This was in accordance with previous studies that demonstrated upregulation of ribosomal biogenesis genes during the transition from qNSCs to aNSCs (Chen et al., 2017; Shin et al., 2015). Among these genes, we found that *Lgals1* (encoding Galectin-1) and *S100a6* were highly expressed in 5 dpi samples (Figure 4A, B and D). We also explored temporal changes in gene expression of Nestin-GFP$^+$ cells after SCI by *Monocle*. Unsupervised clustering by *Monocle* identified covarying genes expressed over pseudotime across the Nestin-GFP$^+$ cells. Pseudotime analysis indicated that *Lgals1* and *S100a6* were upregulated with pseudotime (Figure 4C and E). We verified the reliability of the scRNA-seq results and *Monocle* prediction by immunofluorescence to examine the expression patterns of *Lgals1* and *S100a6* at 0 and 5 pdi. Galectin-1 or S100a6 positive cells were undetectable in the 0 dpi spinal cord, but were detected in 5 pdi Nestin-GFP$^+$ cells (Figure 4F and G). Galectin-1 is a carbohydrate-binding protein that promotes the proliferation of adult NSCs (Sakaguchi et al., 2006; Sakaguchi et al., 2007). S100a6 is a novel marker of NSCs and astrocyte precursors (Yamada and Jinno, 2014) and its expression is increased after injury induced activation of qNSCs in the brain (Llorens-Bobadilla et al., 2015). The high level of expression of these genes in the 5 dpi cells also indicated that some of the qNSCs were activated.

Besides, other lineage-prone markers were also detected in the aNSCs cluster. We detected the increased expression of *Tmsb4x* in the aNSCs cells, which has been reported as a mediator regulating oligodendrocyte differentiation (Figure S5A in Supporting Information) (Santra et al., 2012). Expression of the neural progenitor marker *Fabp7* was also increased in aNSCs cells (Figure 3B), suggesting that the aNSCs possessed an intrinsic neurogenesis ability (Matsumata et al., 2012; Petit et al., 2011).

Our data indicated that after SCI, qNSCs shunted to aNSCs and expressed several lineage-prone markers.

Systematic molecular signatures show Nestin$^+$ cells are activated after SCI

The majority of varied genes among the three clusters were non-coding RNA. Because of the lack of references and unknown functions of these non-coding RNA, we filtered these out and focused on analyzing coding genes. To gain biological insight into these gene expression patterns, we performed GO analyses of the subpopulations of the cells (Figure 5A and B). Upregulated genes in aNSCs were associated with ribosome synthesis and oxidative phosphorylation. Similar results were obtained by Kyoto

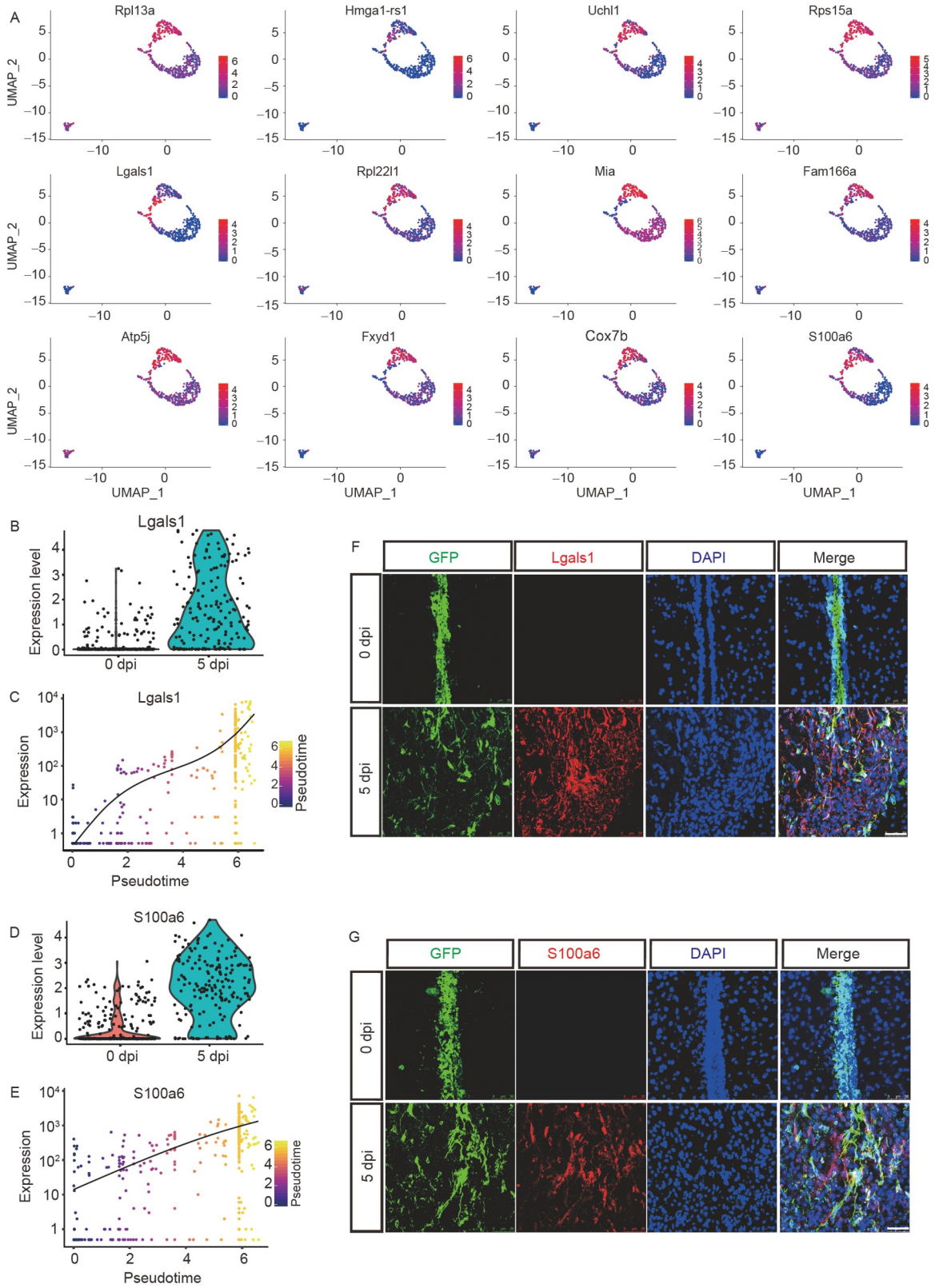

Figure 4 The plasticity of Nestin-GFP^{+} cells after SCI. A, Gene expression profiles of the top 12 marker genes of aNSCs. Most of the genes are involved in oxidative phosphorylation and ribosome synthesis. B and C, Prediction of gene expression pattern of Lgals1 over pseudotime. Vlnplot of expression pattern shows Lgals1 expression probability distributions across clusters qNSCs and aNSCs at 0 and 5 pdi (B). Lgals1 expression pattern over pseudotime (C). D and E, Prediction of the gene expression pattern of S100a6 over pseudotime. Vlnplot of expression pattern shows S100a6 expression probability distributions across clusters qNSCs and aNSCs at 0 and 5 pdi (D). S100a6 expression pattern over pseudotime (E). F and G, Validation of the gene expression patterns of Lgals1 and S100a6 over pseudotime. Immunofluorescence of Lgals1 at 0 and 5 pdi (F). Immunofluorescence of S100a6 at 0 and 5 pdi (G). Scale bars, 50 μm.

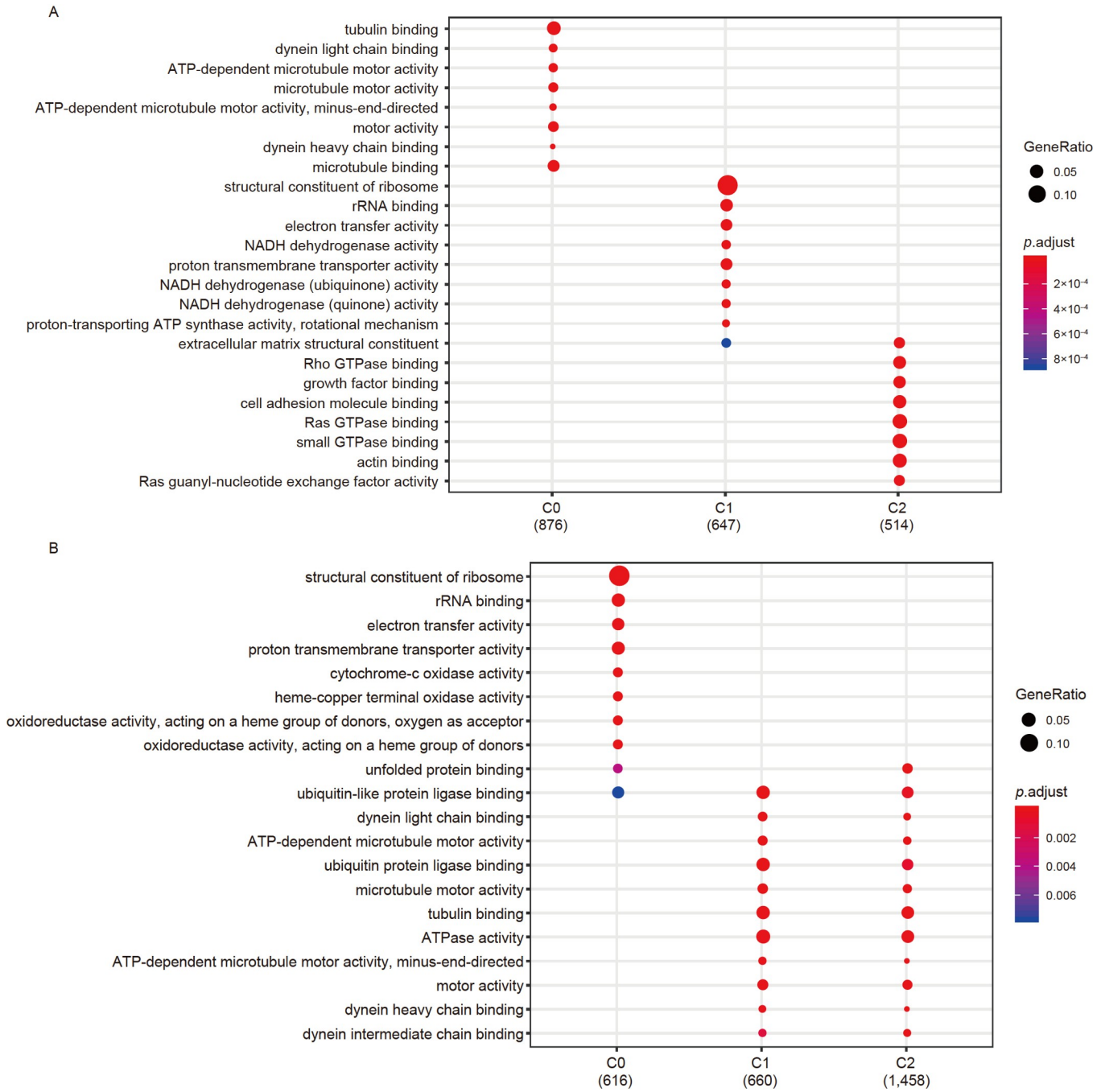

Figure 5 Functional characterization of regulated genes in aNSCs. A, GO term analyses for the cluster-specific upregulated gene biological functions. The top GO terms were selected for each-type-specific gene signature. B, GO term analyses for the cluster-specific downregulated gene biological functions. The top GO terms were selected for each-type-specific gene signature.

Encyclopedia of Genes and Genomes (KEGG) analysis (Figure S4B in Supporting Information). Although the pathways were related to some diseases, the genes were still associated with the oxidative phosphorylation pathway. We also examined the genes that were downregulated in aNSCs, which were associated with microtubule motor activity (Figure 5B). Previous research showed that the oxidative phosphorylation pathway was activated and ribosomal activity increased in adult NSCs during the neurogenesis process (Chen et al., 2017; Llorens-Bobadilla et al., 2015; Shin et al., 2015). To further validate that the Nestin-GFP$^+$ cells were NSCs, we tested the ability of these cells to form neurospheres *in vitro*. Both 0 and 5 pdi Nestin-GFP$^+$ cells gave rise to neutrospheres and could be serially passaged. Neurospheres from 5 pdi Nestin-GFP$^+$ cells appeared faster, and the size of them were larger than the 0 pdi neurospheres (Figure S6 in Supporting Information). These data support that Nestin-GFP$^+$ cells have adult NSCs properties and can

be activated after SCI.

Nestin-GFP$^+$ cells outside the CC are activated during the acute stage after SCI

According to our scRNA-seq data, the expression of *Ccdc153* resembled to the expression of *Foxj1*, but *Ccdc153* expression level was more stable than that of Foxj1 in the 0 and 5 pdi samples (Figure 6A). Several recent scRNA-seq data showed that *Ccdc153* is a specific ependymal cell marker (Chen et al., 2017; Shah et al., 2018). Although Foxj1 is a well-accepted ependymal cell marker, the MCA database showed that it can be found in astrocytes and oligodendrocytes (Figure S7 in Supporting Information). In MCA database, *Ccdc153* expression is more specific in ependymal cell than *Foxj1* (Figure S7 in Supporting Information), suggesting *Ccdc153* is a better marker than Foxj1 to label ependymal cells. To test whether *Ccdc153* can label spinal cord ependymal cells, we detected *Ccdc153* mRNA by using RNAscope. As expected, *Ccdc153* mRNA was located along with the CC at 0 and 5 pdi (Figure 6B and C). Next, we used *Ccdc153* as a marker to separate cells along and outside the CC, and investigated the features of the Nestin-GFP$^+$ cells along the CC at 0 and 5 pdi. MCA analysis showed that the CC cells at 0 and 5 pdi CC cells were quite similar to each other. However, the Nestin-GFP$^+$ cell outside the CC from 5 pdi samples demonstrated several types of cell identities, which suggested that the plasticity of Nestin-GFP$^+$ cell outside the CC were increased after SCI (Figure 6D and E). We carried out neurosphere assay using cells from the 5 pdi spinal cord. Neurospheres derived from 5 pdi cells from outside the CC formed faster and were larger than the neurospheres derived from 0 pdi samples. CC cells are considered as NSCs in spinal cord. To exclude the effects of CC cells in our analysis, we eliminated the CC cells and performed the neurospheres assay by using 5 pdi spinal cord. The number and size of neurospheres were not significantly affected after removing CC cells (Figure S6B in Supporting Information). This result illustrated that Nestin-GFP$^+$ cells outside the CC were activated NSCs. To examine the Nestin-GFP$^+$ cells fate over a short time, we immunostained the 5 pdi spinal cord samples with GFAP and Olig2. The Nestin-GFP$^+$ cells in the CC expressed GFAP. Near the lesion center, some of Nestin-GFP$^+$ cells were stained with GFAP, and only a few of the cells were stained with Olig2 (Figure S6D in Supporting Information), suggesting the Nestin-GFP$^+$ cells have the ability to shunt to astrocytes and oligodendrocytes after SCI *in vivo*.

We then performed GO analysis to further understand the different systematic molecular signatures between Nestin-GFP$^+$ cells outside and within the CC at 5 pdi. The down-regulated genes were involved in cilium organization and cell polarity (Figure 6F and G). Quiescent ependymal cells are enriched in genes involved in ciliogenesis (Ghazale et al., 2019) and polarity related to NSCs differentiation (Arai and Taverna, 2017; Fietz and Huttner, 2011), thus, the down-regulation of ciliogenesis and polarity genes suggested activation of the qNSCs. The upregulated genes were involved in cytoplasmic translation, ribosome biogenesis, cell-substrate adhesion, cell cycle phase transition, oxidative phosphorylation and gliogenesis (Figure 6H and I). These changes are the hallmarks of NSCs activation (Chen et al., 2017; Shin et al., 2015), and their upregulation indicated a shift from qNSCs to aNSCs (Chen et al., 2017; Llorens-Bobadilla et al., 2015; Shin et al., 2015). The GO results suggested that the cells outside the CC, rather than the Nestin-GFP$^+$ cells along with the CC, were the aNSCs after SCI.

DISCUSSION

Understanding the injury induced aNSCs would help us to identify and exploit NSCs sources in the spinal cord. In our study, we purified NSCs from Nestin-GFP transgenic mice and traced the lineage of the immediate progeny of Nestin-GFP$^+$ cells during the acute phase after SCI (Shin et al., 2015; Yamaguchi et al., 2000). Some Nestin-GFP$^+$ cells were scattered outside the CC in the intact spinal cord and Nestin-GFP$^+$ cells were homogeneous before SCI. However, the heterogeneity of these cells increased dramatically at 5 pdi, with the Nestin-GFP$^+$ cells outside the CC acquiring differentiation ability. The cells did not show transcriptional similarity to only one cell type but to multiple cell types. Oxidative phosphorylation related genes and ribosomal subunits related genes were upregulated in these cells. These phenomena are the hallmarks of adult NSCs activation (Beckervordersandforth et al., 2017; Llorens-Bobadilla et al., 2015; Shin et al., 2015; Xu et al., 2013). The G1 to S transition is another important sign of the progression of qNSCs to aNSCs (Dulken et al., 2017; Shin et al., 2015). The genes involved in the cell cycle phase transition and the G1/S checkpoint regulator p53 were highly expressed in aNSCs (Figure S5B in Supporting Information) (Fu et al., 2019; Senturk and Manfredi, 2013). These results suggested that Nestin-GFP$^+$ cells outside the CC escaped from the dormant fate and became aNSCs after SCI.

NSCs in the brain are distinct from ependymal cells (Shah et al., 2018), indicating that there is likely to be another source of NSCs in the spinal cord besides ependymal cells in the CC. Indeed, a potentially novel adult spinal cord NPCs has been discovered in the adult spinal cord, which shares some classic NSC genes with the CC and subventricular zone (Petit et al., 2011). In our study, the Nestin$^+$ cells outside the CC demonstrated the properties of aNSCs, including proliferation and differentiation abilities. Whether Nestin-GFP$^+$

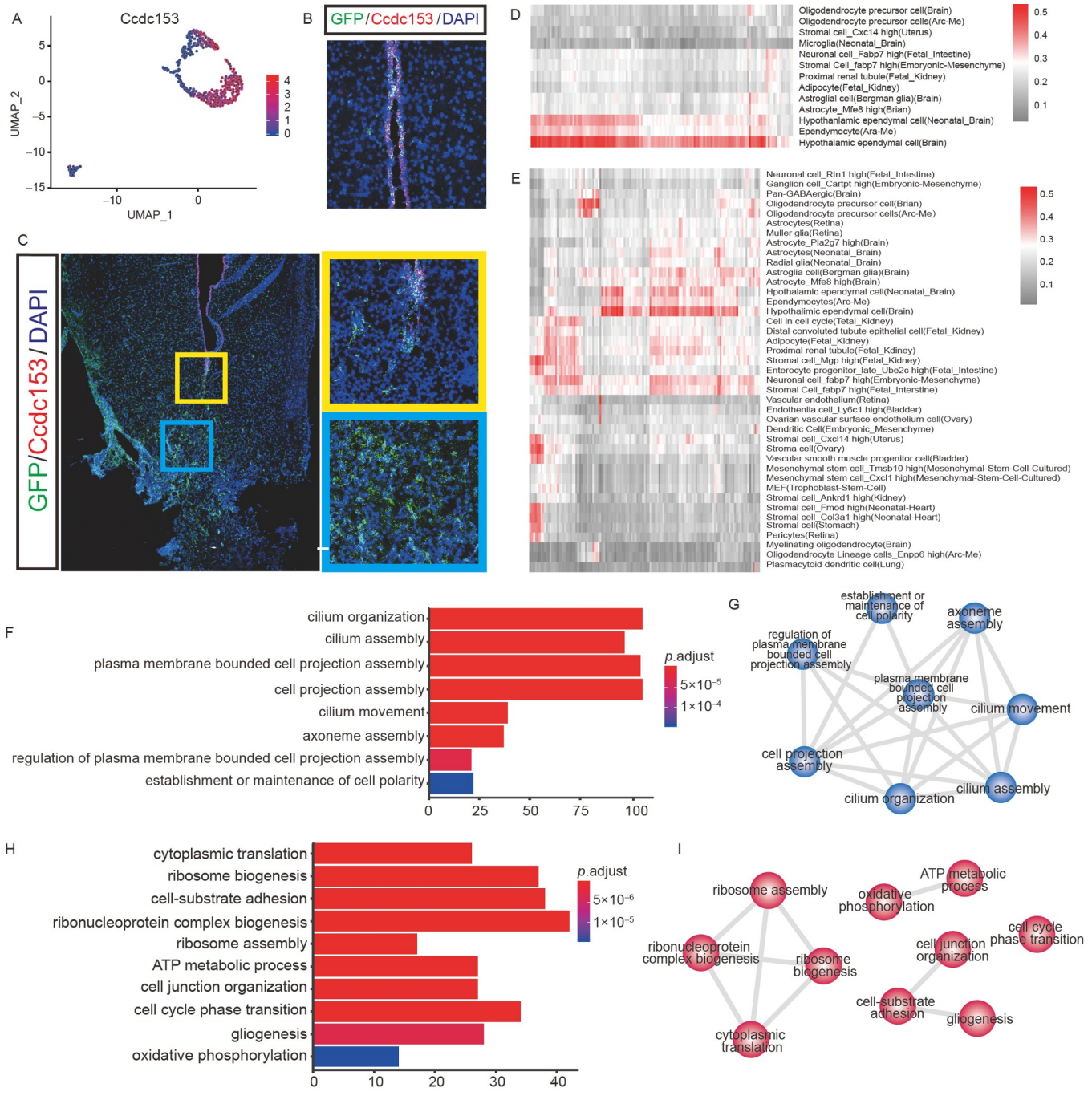

Figure 6 Comparation of molecular mechanisms of Nestin$^+$ cells within/outside the CC during acute stage following SCI. A, Gene expression profiles of *Foxj1* and *Ccdc153*. B and C, Validation of co-labeling for *Gfp* and *Ccdc153* using fluorescence *in situ* hybridization. B shows the result in 0 pdi sample. C shows the result in 5 pdi sample. Scale bars, 50 μm. D and E, MCA analysis of 5 pdi Nestin-GFP$^+$ cells in and out of the CC. Nestin-GFP$^+$ cells in the CC show high similarity to ependymal cells (D). Nestin-GFP$^+$ cells out of CC show intermediate status to other types of cells (E). F and G, Functional GO analysis for downregulated genes (F). The terms that share more than five enriched genes are connected with a line (G). H and I, Functional GO analysis for upregulated genes (H). The terms that share more than five enriched genes are connected with a line (I).

cells outside the CC contribute to the scar forming and whether their ultimate fate is related to the spatial location are interesting questions for further exploration.

We detected some reactive astrocyte markers *Ctnnb1*, *Axin2*, *Plaur*, *Mmp2* and *Mmp3* in our samples (Hara et al., 2017) and found that a few of cells in 5 dpi samples highly expressed these markers (Figure S5C in Supporting Information). Furthermore, these cells highly expressed the aNSC markers. Therefore, we speculated that some Nestin-GFP$^+$ aNSCs captured in the 5 pdi samples probably originated from active astrocytes.

A lack of accurate and efficient approaches has limited the

prospective insights from studies of adult NSCs in the spinal cord. Foxj1, a well-accepted ependymal marker, is a transcription factor involved in motile ciliogenesis (Yu et al., 2008). Previously, the conclusion that ependymal cells in the CC were NSCs was obtained by using human Foxj1-CreER line to trace the fate of NSCs in adult spinal cord. The Foxj1 labeled cells migrated to the injury location and contributed to the scar formation (Barnabé-Heider et al., 2010; Becker et al., 2018; Devaraju et al., 2013; Li et al., 2018a; Muthusamy et al., 2014). However, recently, other groups used a knock-in Foxj1-CreER strain and got faithful ependymal-derived cells which remained the endogenous Foxj1 locus after SCI and their contribution to scar formation was very limited (Muthusamy et al., 2014; Muthusamy et al., 2018; Ren et al., 2017). Foxj1 could also be detected in a subset of neurogenic cells (Jacquet et al., 2009; Li et al., 2018a). In addition, the MCA analysis result showed that Foxj1 can be detected in some astrocytes and oligodendrocytes. Overall, these studies elucidated that Foxj1 is not a specific ependymal marker, and a more specific ependymal marker is therefore required.

In our scRNA-seq analyses, Ccdc153 was specifically detected in ependymal cells, and its expression level was stable in the 0 and 5 pdi samples. We verified the expression of *Ccdc153* by RNAscope, which is a more sensitive technique than immunostaining (Wang et al., 2012). Ccdc153 was exclusively expressed in the CC before and after SCI. Furthermore, several independent groups identified Ccdc153 as a specific ependymal marker (Chen et al., 2017; Shah et al., 2018). Therefore, Ccdc153 is a better ependymal cells marker than Foxj1, and Ccdc153-CreER can be a better tool to analyze ependymal cell features in the future.

Our scRNA-seq data captured the transition status of aNSCs, which demonstrated that activated Nestin-GFP$^+$ cells started to express genes that specific to astrocytes, radial glia cells, neurons and oligodendrocytes. To further test the NSCs properties of these cells, we performed differentiation assays. After 7 d of differentiation culture, 19.67%±1.45% of cells per visual field were positively stained for the astrocytes marker GFAP and 3.63%±0.23% of cells per visual field were positively stained for the newborn neuron marker Tuj-1, confirming that Nestin-GFP$^+$ cells were aNSCs that could be isolated from injured adult mouse spinal cords and that have the potential to differentiate into neurons in vitro (Figure S6C in Supporting Information) (Li et al., 2018b; Li et al., 2019). We compared the 0 and 5 pdi transcriptomic profiles with a previously published developmental dataset of neural progenitors. The transcriptomic profiles from the 5 pdi Nestin-GFP$^+$ cells showed a significant correlation with the embryonic neural progenitor dataset (Figure S6E in Supporting Information) (Delile et al., 2019). Previous research suggested that NSCs in the spinal cord only had a glial fate, and no neuronal fate *in vivo*. Although the immature neuron marker DCX and mature neuron marker Tubb3 were rarely detected in Nestin-GFP$^+$ cells *in vivo*, our data showed that neural progenitor marker Fabp7 was increased in aNSCs. We cannot rule out the possibility that the aNSCs can develop into neurons. Because Nestin was only expressed in NSCs/NPCs and mature neurons do not continue expressing the protein, we were unable to capture the immature or mature neuron in our mice. Further studies are therefore needed to isolate Nestin$^+$ cells from Nes-CreERT2 mice to determine whether the aNSCs can turn into neurons.

Overall, our single-cell transcriptome analysis revealed a novel group of Nestin-GFP$^+$ cell located outside the CC in the adult spinal cord. Instead of the quiescent feature of Nestin-GFP$^+$ cells in the CC, these cells showed notable aNSCs properties, and were highly heterogenous after SCI. This study paves the way for further dissection of Nestin$^+$ cells following SCI, and may lead to improved approaches for regenerative treatment after SCI.

MATERIALS AND METHODS

Surgical procedures

All surgeries were performed under the Chinese Ministry of Public Health Guidelines and US National Institutes of Health Guidelines for the care and use of animals. Adult mice of both sexes (8–10 months of age) were used for experiments. Laminectomy of a single vertebra was performed and 1 mm midline incision was made at the level of T8–T10 of the spinal cord. All animals received analgesic prior to wound closure and every 12 h for at least 48 h post-injury. After the operation, mice received antibiotics treatment for 3 d (Shen et al., 2020; Xue et al., 2021).

Fluorescence-Nestin cell sorting

Nestin-GFP transgenic mouse line (C57BL/6) was used for FACS (BD FACSAria II, USA). The cells expressed GFP under the Nestin promoter (Yamaguchi et al., 2000). To obtain the GFP cells, T6–T10 of the spinal cord were collected from 6- to 8-week old mice, chopped into ~1 mm^3 pieces and incubated with Accutase (Sigma-Aldrich, USA) for 15 min. The reaction was stopped with equal volume of phosphate-buffered saline (PBS) and the mixture was then filtered with 40 μm nylon cell strainer to obtain a single cell suspension. Cellular debris and dead cells were removed by centrifugation at 500×*g* for 3 min. The pellet was dissolved to a concentration of 1,000 cells per μm in DMEM: F12 medium (Gibco, USA) containing N2 supplement (Life Technologies, USA). FACS was performed using a 488 nm laser for GFP excitation and 530/30 nm for filtering. Filtered cells were stored in 96-well plates containing lysis buffer (0.2% (vol/vol) Triton X-100 and 2 U μL^{-1} RNase inhibitor).

Immunohistochemistry

Spinal cords were perfusion-fixed with 4% paraformaldehyde (PFA) at 4°C overnight. Then the samples were incubated in 30% sucrose (Vetec, USA), and embedded in OCT compound (Sakura, USA). Sections (15 μm) were prepared using a cryostat (Leica, Germany) and stored at −80°C until further use. Sections were blocked with 5% bovine serum albumin (Sori) with 0.2% Triton X-100 (Sigma-Aldrich) for 1 h at room temperature. Then, the sections were incubated with primary antibody (1:500) at 4°C overnight. The primary antibodies used are listed in Table S1 in Supporting Information. After three rinses in PBS, sections were incubated with Alexa Fluor (488, 568, 648)-conjugated secondary antibodies (1:500; Invitrogen, USA) for 1 h incubation at room temperature. Slides were imaged by confocal microscope (Leica SP8).

In situ hybridization

Nestin-GFP mice (8–10 weeks old) were euthanized with an overdose of sodium pentobarbital and then perfused with PBS and then spinal cords were incubated with 4% PFA for 24 h and subsequently equilibrated in 30% sucrose at 4°C for 24 h. The samples were imbedded in OCT compound for storage at −80°C. Frozen sections (10 μm) were cut and RNAscope (ACD) was used for *in situ* hybridization following the manufacturer's protocol. Slides were imaged by confocal microscopy (Leica SP8).

BrdU and BrdU-labeled section immunostaining

BrdU (Sigma-Aldrich) was dissolved in PBS. SCI mice were administered BrdU by intraperitoneal injections every 6 h at 100 mg kg^{-1} per injection for 3 d, starting immediately after SCI surgery. Frozen sections were prepared as described above. DNA hydrolysis step was required before standard immunostaining process. Sections were incubated in 1 mol L^{-1} HCL for 30 min at 37°C, neutralized with 0.1 mol L^{-1} sodium borate buffer for 10 min at room temperature, and then washed three times with PBS for approximately 5 min each. The sections were then subjected to standard immunostaining protocols.

Workflows of Smart-seq2

Smart-seq2 for transcriptome analysis of single cells was adapted as described previously (Picelli et al., 2014). Briefly, the procedure includes the following seven steps: (i) cell lysis, (ii) reverse transcription, (iii) template switching, (iv) PCR preamplification of cDNA, (v) tagmentation by Tn5, (vi) gap repair, enrichment PCR and PCR purification, and (vii) sequencing. cDNA amplification of GFP^+ cells was involved 22 PCR cycles. Tagmentation was using True-Prep™DNA Library Prep Kit V2 for Illumina® (Vazyme, Nanjing, China). Sequencing was performed using Illumina NextSeq 500 system. Each cell library was sequenced to an average depth of 2 million total reads.

NSC cultures and differentiation

Spinal cord cells were dissociated and neurosphere cultures were performed according to previously described protocols (Meletis et al., 2008). Cells were isolated from the spinal cords of three mice in each group. Single recombined neurospheres were picked, dissociated, and plated in a 24-well plate. Clonally derived secondary neurospheres were collected for continuous passaging and then for plating in poly-D-lysine-coated plate. After 4 h in NSC culture condition, immunocytochemistry was performed with antibodies described in the Supplemental Information. For differentiation, neurospheres were dissociated to single cells and resuspended in adhesion medium containing 10% FBS. After 24 h culture, the cells were plated on poly-D-lysine-coated plate by differentiation medium containing 2% B27 in DMEM/F12 medium.

Single cell RNA-seq processing

BCL basecall files were generated from the Illumina MiSeq instruments. We used bcl2fastq (Version 1.8.4) program to combine these per-cycle BCL files from a run and translates them into FASTQ files. At the same time as converting, bcl2fastq also separated multiplexed samples into single cells according to the barcodes. Sequencing quality and adapter-contamination were checked by FastQC. Raw sequencing reads were trimmed to remove the adapter-contaminated and low-quality reads using Trimmomatic (Version 0.36). Gene expression of each single cells was quantified using Salmon (version 0.8.1) with parameters "-l A –seqBias –gcBias –posBias". Finally, all read counts of each genes of each single cell were aggregated to generate gene expression counts table.

R package Seurat (version 3.1.1) was used for data preparation and downstream analysis (Butler et al., 2018; Stuart et al., 2019). rRNA genes have been removed because they were irrelevant to the study. Cells with <2,000 features or >12,000 features have been filtered out because too low or too high gene features are more likely to be incomplete cell samples or multiple cell samples, respectively. In addition, cells with a high percentage (above 30%) of mitochondrial gene expression, regarding as dying cells, have also been removed from the expression matrix. Based on the PCA results, the first eight dimensions are selected for further clustering. Default functions from the Seurat package have been used to find neighbors and cluster cells with a resolu-

tion of 0.2. All clustering results were visualized by using the UMAP dimension reduction technique. GO and KEGG analysis have been done with R package clusterProfiler (Yu et al., 2012). The cell sampled in cluster 2, which was identified as epithelia, was excluded from further study on CC and pseudotime analysis.

To investigate the gene expression pattern around CC and away from the CC, cell samples without cluster 2 cells have been divided into four groups corresponding to Ccdc153 expression level and time points. Specifically, the cutoff for Ccdc153 expression level was 0.1 transcripts per million (TPM) which was chosen confidently based on the distribution of the gene expression level across all samples.

Pseudotime analysis was carried out using new version of Monocle3 R package has be utilized and default parameters were applied (Trapnell et al., 2014).

Correlation with a previously published embryonic dataset

We aggregated the single-cell data to pseudobulk data, and then normalized the 0 and 5 pdi datasets. The GO ranked gene expression terms were shown as log-transformed fold changes. These were derived by comparing our 0 and 5 pdi Nestin-GFP$^+$ cells datasets with that of embryonic day 9.5–13.5 neural progenitors (Delile et al., 2019).

Data availability

The datasets generated and analyzed during the current study are available in the BIGD (National Genomics Data Center, Beijing Institute of Genomics, Chinese Academy of Sciences) database under the bioproject accession code: PRJCA003115.

Compliance and ethics *The author(s) declare that they have no conflict of interest.*

Acknowledgements *This work was supported by the National Natural Science Foundation of China (81891002 and 81891001), the Strategic Priority Research Program of the Chinese Academy of Sciences (XDA16040700), the National Key Research and Development Program of China (2017YFA0104701, 2017YFA0104704 and 2016YFC1101501), and Jiangsu Key Research and Development Program (BE2018664).*

References

Arai, Y., and Taverna, E. (2017). Neural progenitor cell polarity and cortical development. Front Cell Neurosci 11, 384.

Barnabé-Heider, F., Göritz, C., Sabelström, H., Takebayashi, H., Pfrieger, F.W., Meletis, K., and Frisén, J. (2010). Origin of new glial cells in intact and injured adult spinal cord. Cell Stem Cell 7, 470–482.

Becker, C.G., Becker, T., and Hugnot, J.P. (2018). The spinal ependymal zone as a source of endogenous repair cells across vertebrates. Prog Neurobiol 170, 67–80.

Beckervordersandforth, R., Ebert, B., Schäffner, I., Moss, J., Fiebig, C., Shin, J., Moore, D.L., Ghosh, L., Trinchero, M.F., Stockburger, C., et al. (2017). Role of mitochondrial metabolism in the control of early lineage progression and aging phenotypes in adult hippocampal neurogenesis. Neuron 93, 560–573.e6.

Bernal, A., and Arranz, L. (2018). Nestin-expressing progenitor cells: function, identity and therapeutic implications. Cell Mol Life Sci 75, 2177–2195.

Butler, A., Hoffman, P., Smibert, P., Papalexi, E., and Satija, R. (2018). Integrating single-cell transcriptomic data across different conditions, technologies, and species. Nat Biotechnol 36, 411–420.

Cawsey, T., Duflou, J., Weickert, C.S., and Gorrie, C.A. (2015). Nestin-positive ependymal cells are increased in the human spinal cord after traumatic central nervous system injury. J Neurotrauma 32, 1393–1402.

Chen, R., Wu, X., Jiang, L., and Zhang, Y. (2017). Single-cell RNA-seq reveals hypothalamic cell diversity. Cell Rep 18, 3227–3241.

Delile, J., Rayon, T., Melchionda, M., Edwards, A., Briscoe, J., and Sagner, A. (2019). Single cell transcriptomics reveals spatial and temporal dynamics of gene expression in the developing mouse spinal cord. Development 146, dev173807.

Devaraju, K., Barnabé-Heider, F., Kokaia, Z., and Lindvall, O. (2013). FoxJ1-expressing cells contribute to neurogenesis in forebrain of adult rats: Evidence from *in vivo* electroporation combined with *piggyBac* transposon. Exp Cell Res 319, 2790–2800.

Dulken, B.W., Leeman, D.S., Boutet, S.C., Hebestreit, K., and Brunet, A. (2017). Single-cell transcriptomic analysis defines heterogeneity and transcriptional dynamics in the adult neural stem cell lineage. Cell Rep 18, 777–790.

Fietz, S.A., and Huttner, W.B. (2011). Cortical progenitor expansion, self-renewal and neurogenesis—A polarized perspective. Curr Opin NeuroBiol 21, 23–35.

Fu, X., Wu, S., Li, B., Xu, Y., and Liu, J. (2019). Functions of p53 in pluripotent stem cells. Protein Cell 11, 71–78.

Ghazale, H., Ripoll, C., Leventoux, N., Jacob, L., Azar, S., Mamaeva, D., Glasson, Y., Calvo, C.F., Thomas, J.L., Meneceur, S., et al. (2019). RNA profiling of the human and mouse spinal cord stem cell niches reveals an embryonic-like regionalization with MSX1$^+$ roof-plate-derived cells. Stem Cell Rep 12, 1159–1177.

Göritz, C., Dias, D.O., Tomilin, N., Barbacid, M., Shupliakov, O., and Frisén, J. (2011). A pericyte origin of spinal cord scar tissue. Science 333, 238–242.

Grün, D., and van Oudenaarden, A. (2015). Design and analysis of single-cell sequencing experiments. Cell 163, 799–810.

Habib, N., Li, Y., Heidenreich, M., Swiech, L., Avraham-Davidi, I., Trombetta, J.J., Hession, C., Zhang, F., and Regev, A. (2016). Div-seq: single-nucleus RNA-Seq reveals dynamics of rare adult newborn neurons. Science 353, 925–928.

Hamilton, L.K., Truong, M.K.V., Bednarczyk, M.R., Aumont, A., and Fernandes, K.J.L. (2009). Cellular organization of the central canal ependymal zone, a niche of latent neural stem cells in the adult mammalian spinal cord. Neuroscience 164, 1044–1056.

Hara, M., Kobayakawa, K., Ohkawa, Y., Kumamaru, H., Yokota, K., Saito, T., Kijima, K., Yoshizaki, S., Harimaya, K., Nakashima, Y., et al. (2017). Interaction of reactive astrocytes with type I collagen induces astrocytic scar formation through the integrin-N-cadherin pathway after spinal cord injury. Nat Med 23, 818–828.

Hugnot, J.P., and Franzen, R. (2011). The spinal cord ependymal region: a stem cell niche in the caudal central nervous system. Front Biosci 16, 1044–1059.

Jacquet, B.V., Salinas-Mondragon, R., Liang, H., Therit, B., Buie, J.D., Dykstra, M., Campbell, K., Ostrowski, L.E., Brody, S.L., and Ghashghaei, H.T. (2009). FoxJ1-dependent gene expression is required for differentiation of radial glia into ependymal cells and a subset of astrocytes in the postnatal brain. Development 136, 4021–4031.

Klein, T., Ling, Z., Heimberg, H., Madsen, O.D., Heller, R.S., and Serup, P. (2003). Nestin is expressed in vascular endothelial cells in the adult human pancreas. J Histochem Cytochem 51, 697–706.

Li, X., Zhao, Y., Cheng, S., Han, S., Shu, M., Chen, B., Chen, X., Tang, F.,

Wang, N., Tu, Y., et al. (2017). Cetuximab modified collagen scaffold directs neurogenesis of injury-activated endogenous neural stem cells for acute spinal cord injury repair. Biomaterials 137, 73–86.
Li, X., Floriddia, E.M., Toskas, K., Chalfouh, C., Honore, A., Aumont, A., Vallières, N., Lacroix, S., Fernandes, K.J.L., Guérout, N., et al. (2018a). FoxJ1 regulates spinal cord development and is required for the maintenance of spinal cord stem cell potential. Exp Cell Res 368, 84–100.
Li, X., Fan, C., Xiao, Z., Zhao, Y., Zhang, H., Sun, J., Zhuang, Y., Wu, X., Shi, J., Chen, Y., et al. (2018b). A collagen microchannel scaffold carrying paclitaxel-liposomes induces neuronal differentiation of neural stem cells through Wnt/β-catenin signaling for spinal cord injury repair. Biomaterials 183, 114–127.
Li, X., Liu, D., Xiao, Z., Zhao, Y., Han, S., Chen, B., and Dai, J. (2019). Scaffold-facilitated locomotor improvement post complete spinal cord injury: Motor axon regeneration versus endogenous neuronal relay formation. Biomaterials 197, 20–31.
Llorens-Bobadilla, E., Zhao, S., Baser, A., Saiz-Castro, G., Zwadlo, K., and Martin-Villalba, A. (2015). Single-cell transcriptomics reveals a population of dormant neural stem cells that become activated upon brain injury. Cell Stem Cell 17, 329–340.
Luo, Y., Coskun, V., Liang, A., Yu, J., Cheng, L., Ge, W., Shi, Z., Zhang, K., Li, C., Cui, Y., et al. (2015). Single-cell transcriptome analyses reveal signals to activate dormant neural stem cells. Cell 161, 1175–1186.
Matsumata, M., Sakayori, N., Maekawa, M., Owada, Y., Yoshikawa, T., and Osumi, N. (2012). The effects of Fabp7 and Fabp5 on postnatal hippocampal neurogenesis in the mouse. Stem Cell 30, 1532–1543.
Meletis, K., Barnabé-Heider, F., Carlén, M., Evergren, E., Tomilin, N., Shupliakov, O., and Frisén, J. (2008). Spinal cord injury reveals multilineage differentiation of ependymal cells. PLoS Biol 6, e182.
Mirzadeh, Z., Merkle, F.T., Soriano-Navarro, M., Garcia-Verdugo, J.M., and Alvarez-Buylla, A. (2008). Neural stem cells confer unique pinwheel architecture to the ventricular surface in neurogenic regions of the adult brain. Cell Stem Cell 3, 265–278.
Muthusamy, N., Vijayakumar, A., Cheng Jr, G., and Ghashghaei, H.T. (2014). A knock-in *Foxj1*$^{CreERT2::GFP}$ mouse for recombination in epithelial cells with motile cilia. Genesis 52, 350–358.
Muthusamy, N., Brumm, A., Zhang, X., Carmichael, S.T., and Ghashghaei, H.T. (2018). Foxj1 expressing ependymal cells do not contribute new cells to sites of injury or stroke in the mouse forebrain. Sci Rep 8, 1766.
Nomura, T., Göritz, C., Catchpole, T., Henkemeyer, M., and Frisén, J. (2010). EphB signaling controls lineage plasticity of adult neural stem cell niche cells. Cell Stem Cell 7, 730–743.
Paniagua-Torija, B., Norenberg, M., Arevalo-Martin, A., Carballosa-Gautam, M.M., Campos-Martin, Y., Molina-Holgado, E., and Garcia-Ovejero, D. (2018). Cells in the adult human spinal cord ependymal region do not proliferate after injury. J Pathol 246, 415–421.
Petit, A., Sanders, A.D., Kennedy, T.E., Tetzlaff, W., Glattfelder, K.J., Dalley, R.A., Puchalski, R.B., Jones, A.R., and Roskams, A.J. (2011). Adult spinal cord radial glia display a unique progenitor phenotype. PLoS ONE 6, e24538.
Picelli, S., Faridani, O.R., Björklund, A.K., Winberg, G., Sagasser, S., and Sandberg, R. (2014). Full-length RNA-seq from single cells using Smart-seq2. Nat Protoc 9, 171–181.
Ren, Y., Ao, Y., O'Shea, T.M., Burda, J.E., Bernstein, A.M., Brumm, A.J., Muthusamy, N., Ghashghaei, H.T., Carmichael, S.T., Cheng, L., et al. (2017). Ependymal cell contribution to scar formation after spinal cord injury is minimal, local and dependent on direct ependymal injury. Sci Rep 7, 41122.
Sabelström, H., Stenudd, M., and Frisén, J. (2014). Neural stem cells in the adult spinal cord. Exp Neurol 260, 44–49.
Sakaguchi, M., Shingo, T., Shimazaki, T., Okano, H.J., Shiwa, M., Ishibashi, S., Oguro, H., Ninomiya, M., Kadoya, T., Horie, H., et al. (2006). A carbohydrate-binding protein, Galectin-1, promotes proliferation of adult neural stem cells. Proc Natl Acad Sci USA 103, 7112–7117.
Sakaguchi, M., Imaizumi, Y., and Okano, H. (2007). Expression and function of galectin-1 in adult neural stem cells. Cell Mol Life Sci 64, 1254–1258.
Santra, M., Chopp, M., Zhang, Z.G., Lu, M., Santra, S., Nalani, A., Santra, S., and Morris, D.C. (2012). Thymosin beta4 mediates oligodendrocyte differentiation by upregulating p38 MAPK. Glia 60, 1826–1838.
Senturk, E., and Manfredi, J.J. (2013). p53 and cell cycle effects after DNA damage. In: Deb, S., and Deb, S., eds. p53 Protocols. Methods in Molecular Biology (Methods and Protocols). Totowa: Humana Press. 49–61.
Shah, P.T., Stratton, J.A., Stykel, M.G., Abbasi, S., Sharma, S., Mayr, K.A., Koblinger, K., Whelan, P.J., and Biernaskie, J. (2018). Single-cell transcriptomics and fate mapping of ependymal cells reveals an absence of neural stem cell function. Cell 173, 1045–1057.e9.
Shen, H., Wu, S., Chen, X., Xu, B., Ma, D., Zhao, Y., Zhuang, Y., Chen, B., Hou, X., Li, J., et al. (2020). Allotransplantation of adult spinal cord tissues after complete transected spinal cord injury: Long-term survival and functional recovery in canines. Sci China Life Sci 63, 1879–1886.
Shin, J., Berg, D.A., Zhu, Y., Shin, J.Y., Song, J., Bonaguidi, M.A., Enikolopov, G., Nauen, D.W., Christian, K.M., Ming, G., et al. (2015). Single-cell RNA-seq with waterfall reveals molecular cascades underlying adult neurogenesis. Cell Stem Cell 17, 360–372.
Stuart, T., Butler, A., Hoffman, P., Hafemeister, C., Papalexi, E., Mauck Iii, W.M., Hao, Y., Stoeckius, M., Smibert, P., and Satija, R. (2019). Comprehensive integration of single-cell data. Cell 177, 1888–1902.e21.
Trapnell, C., Cacchiarelli, D., Grimsby, J., Pokharel, P., Li, S., Morse, M., Lennon, N.J., Livak, K.J., Mikkelsen, T.S., and Rinn, J.L. (2014). The dynamics and regulators of cell fate decisions are revealed by pseudotemporal ordering of single cells. Nat Biotechnol 32, 381–386.
Wang, F., Flanagan, J., Su, N., Wang, L.C., Bui, S., Nielson, A., Wu, X., Vo, H.T., Ma, X.J., and Luo, Y. (2012). RNAscope. J Mol Diagn 14, 22–29.
Xu, X., Duan, S., Yi, F., Ocampo, A., Liu, G.H., and Izpisua Belmonte, J.C. (2013). Mitochondrial regulation in pluripotent stem cells. Cell Metab 18, 325–332.
Xue, X., Shu, M., Xiao, Z., Zhao, Y., Li, X., Zhang, H., Fan, Y., Wu, X., Chen, B., Xu, B., et al. (2021). Lineage tracing reveals the origin of Nestin-positive cells are heterogeneous and rarely from ependymal cells after spinal cord injury. Sci China Life Sci doi: 10.1007/s11427-020-1901-4.
Yamada, J., and Jinno, S. (2014). S100A6 (calcyclin) is a novel marker of neural stem cells and astrocyte precursors in the subgranular zone of the adult mouse hippocampus. Hippocampus 24, 89–101.
Yamaguchi, M., Saito, H., Suzuki, M., and Mori, K. (2000). Visualization of neurogenesis in the central nervous system using nestin promoter-GFP transgenic mice. Neuroreport 11, 1991–1996.
Yu, G., Wang, L.G., Han, Y., and He, Q.Y. (2012). clusterProfiler: an R package for comparing biological themes among gene clusters. OMICS 16, 284–287.
Yu, X., Ng, C.P., Habacher, H., and Roy, S. (2008). Foxj1 transcription factors are master regulators of the motile ciliogenic program. Nat Genet 40, 1445–1453.

SUPPORTING INFORMATION

The supporting information is available online at https://doi.org/10.1007/s11427-020-1930-0. The supporting materials are published as submitted, without typesetting or editing. The responsibility for scientific accuracy and content remains entirely with the authors.